Macroscopic sheets of hydrogen boride and their spectroscopic evaluation

Kazuki Yamaguchi [ORCID],[1] Masahito Niibe [ORCID],[1] Xiaoni Zhang,[1] Toshihide Sumi,[1] Masafumi Horio [ORCID],[1] Yasunobu Ando,[2]
Jun-ichi Yamaura [ORCID],[1] Eiken Nakamura,[3] Kiyohisa Tanaka,[3,4] Takahiro Kondo [ORCID],[5] and Iwao Matsuda [ORCID][1]

[1]*Institute for Solid State Physics (ISSP), The University of Tokyo, Kashiwa, Chiba 277-8581, Japan*
[2]*CD-FMat, National Institute of Advanced Industrial Science and Technology (AIST), Tsukuba, Ibaraki 305-8560, Japan*
[3]*Institute for Molecular Science, Myodaijicho, Okazaki, Aichi 444-8585, Japan*
[4]*The Graduate University for Advanced Studies, Myodaijicho, Okazaki, Aichi 444-8585, Japan*
[5]*Institute of Pure and Applied Sciences, University of Tsukuba, Tsukuba, Ibaraki 305-8573, Japan*

Macroscopic sheets of hydrogen boride (HB) were fabricated by annealing microflakes, synthesized after the ion-exchange reaction. The sheets were centimeters wide and a micrometer thick. Handy and easy handling of the sheets has allowed us to conduct spectroscopic evaluations over various photon energy ranges. X-ray absorption spectra at the B K-shell absorption edge were obtained; the narrow spectral peaks were reproduced in theoretical simulations, revealing bonding characters between the H and B atoms. The macroscopic fabrication demonstrated in the present research offers a bottom-up approach toward real-world applications of these HB sheets.

I. INTRODUCTION

Varieties of two-dimensional (2D) materials have been designed, synthesized, and characterized, showing a multitude of different physical and chemical properties. A layer of graphene is semimetallic with characteristic electronic states in the shape of Dirac cones, whereas those of transition metal dichalcogenides are semiconducting materials for which energy gaps depend on their composition. Such 2D materials have nowadays been categorized into libraries and their functionalities investigated for future technology [1,2]. For efficient performance in applications, the dimensions of these materials, i.e., thickness or area, have become an issue. For example, fine powders are suitable for catalysts, whereas large sheets are required in (opto)electronic devices [3]. Size control has been achieved through methods such as cutting, cleaving, exfoliating, and pulverizing of bulk samples of van der Waals crystals, which are typical sources of 2D materials. Such top-down methodologies are easily scalable and cost-effective but based on ready-made bulk crystals. In contrast, novel 2D materials have been grown on substrates or synthesized into nanometer-scale flakes. Size control has been challenged by the bottom-up approach but it typically has high production costs, low yield, and limited scalability, making mass production difficult.

Recently, researchers have focused on boron materials and reported varieties of 2D elemental allotropes and compounds [4]. A layer of hydrogen boride (HB), so-called "borophane", has been reported to form on a metal substrate or chemically synthesized in a free-standing manner [5–10]. Because of the polymorphism of the boron networks, there are abundance of the HB structures [5–17]. The diversity of physical and chemical properties offers a variety of possible applications, proposed and examined in various fields of catalysis and (opto)electronics [18–28]. Currently, a free-standing HB sheet of the honeycomb-lattice type [see Fig. 1(a)], has been the focus of attention in both academia and industry [29]. This is mainly because the material can be prepared simply by the ion-exchange reaction at room temperature and displays several functionalities, such as hydrogen transfer [24] and C-C coupling reaction [23]. The HB sheets are obtained as a powder of micrometer-scale flakes [7,9]; see Fig. 1(b) and Appendix. To be ready for wide applications, an investigation of the size control toward much larger scale is warranted.

In the present research, we fabricated macroscopic sheets of hydrogen boride using the postannealing treatment of powder synthesized from the ion-exchange reaction. The HB sheets have areas up to a few square centimeters and thicknesses of micrometers. Electronic states, as evaluated by spectroscopy, were consistent with those of HB powders, reported previously [14]. These macroscopic sheets have allowed us to perform precise x-ray absorption spectroscopy (XAS). The experimental spectra at the B K-edge showed good agreement with the simulated spectra, giving clear orbital assignments of the electronic states. The macroscopic HB sheets and the fabrication method, developed in the present research, may be useful in several fields of technology.

II. EXPERIMENTAL

The research was conducted in steps commencing with synthesis, then spectroscopic evaluation, and finally calculation.

A. Synthesis

The fabrication of the macroscopic HB sheets was made by extending the ion-exchange reaction method [7]. To begin with, a 2.0 g powder of the MgB_2 crystals (99%, Rare Metallic Co. Ltd. Tokyo, Japan) was mixed with an ion-exchange resin
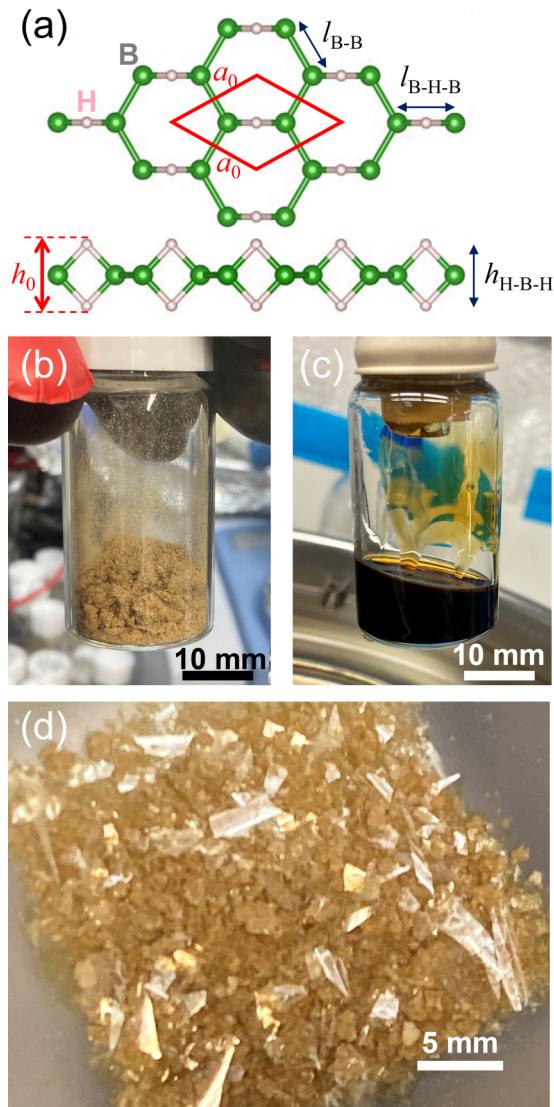
FIG. 1. Varieties of HB sheet samples. (a) A structure model of the honeycomb-lattice type HB sheet. The structural parameters are defined in the figure. Photograph images of (b) the powder sample, (c) the HB-containing solution, and (d) the macroscopic HB sheets.

(Amberlite IR120B H HG, Organo Corp., Tokyo, Japan) in a 300 mL acetonitrile liquid (99.5%, JIS special grade, FU-JIFILM Wako Pure Chemical Corp, Osaka, Japan) under an Ar atmosphere [7]. After removing the resin, the unreacted mother material MgB_2, and byproducts either boric acid or boron oxide by filtration, we confirmed the fabrication of the HB sheets by Fourier transform infrared spectroscopy and x-ray diffraction (XRD), as reported previously [7]. In the present research, we extensively added the following procedures. The sample filtrate was annealed at 80 °C to vaporize the acetonitrile until the sample volume became less than 20 ml. Through the removal of byproducts by filtration, we obtained a solution that contained the HB sheets [Fig. 1(c)]. The 1 ml solution was mixed with 10 ml acetonitrile liquid and it is subsequently heated in vacuum at 80 °C to vaporize the solvent. When the solvent is vaporized to some extent, the solution has viscosity and it sticks on a bottle wall or on a

substrate. At this stage, the annealing temperature is raised up to 100 °C and the solvent is completely vaporized. As a consequence, the HB sheets remains on the wall surface (substrate) and the heating condition is kept for several hours. The situation is shown in Fig. 7 in Appendix and the HB sheet, shown in Fig. 1(d), are obtained by peeling them off from the wall surface (substrate). The sheet sizes in the figure are ~cm² in area and ~1 μm in thickness. One can, in principle, prepare the HB sheet in any size by choosing the appropriate size of a substrate and by making the careful detachment. The density of a HB or borophane sheet was experimentally evaluated to be 1.16 ± 0.23 g/cm³, which is consistent with what was expected (1.4 g/cm³) from the structure model [7,14,24]; see Fig. 1(a) and previous report (1.26 g/cm³) [30]. Notably, this density value is much smaller than that of graphite (2.25 g/cm³). Moreover, the macroscopic sheet is millimeter sized, which is one hundred thousand times larger in surface area than that of the microscopic flakes that have been synthesized [7]. The sheets are convenient to handle and easily broken into pieces.

The present fabrication procedure has an advantage—the macroscopic HB sheets can be prepared on a variety of substrates. This is achieved simply by soaking a substrate in a HB-containing solution [Fig. 1(c)], followed by the stepwise annealing described above. We have confirmed the availability on typical substrates, such as a Si wafer (see Appendix) and a Ni wire mesh [Fig. 4(a) below].

B. X-ray diffraction

An XRD pattern of the macroscopic HB sheet [Fig. 1(d)] was obtained using a diffractometer, Rigaku R-AXIS RAPID II. The x-ray source was the MoKα line, generated at 40 kV and 30 mA. The HB sheet, dispersed in oil, was scooped up with a sample holder and fixed by its own surface tension. The XRD measurement was taken at room temperature.

C. Spectroscopic evaluations

Measurements of visible–ultraviolet (VIS-UV) spectroscopy was performed using the UH4150 spectrophotometer from the Hitachi High-Tech Corporation. A VIS-UV spectrum was obtained in the transmission geometry. The measurement sample was placed perpendicular to the incident light. Experiments of XAS were made in beamline BL5B at the UltraViolet Synchrotron Orbital Radiation (UVSOR) [31]. The sample was placed perpendicular to the incident direction of the light, and the light was linearly polarized for the measurement. XAS spectra were recorded with two types of signal detections: transmission and total electron yield (TEY) methods [32]. The spectral information obtained by the two methods are concomitant; the transmission signal is bulk sensitive, whereas the signal by the TEY method is surface sensitive. The combination provides comprehensive information on a sample. All measurements were taken at room temperature.

D. Spectral calculation

The spectral simulation was conducted using the computer code Cambridge Serial Total Energy Package (CASTEP), which is a program of the *ab initio* quantum-mechanical
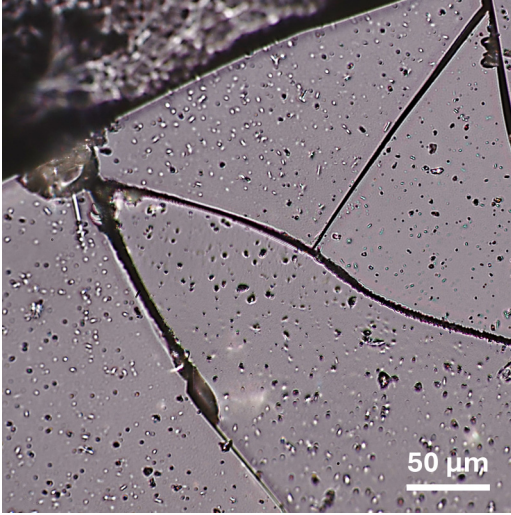
FIG. 2. Image of a macroscopic HB sheet, observed using an optical microscope.

calculation, based on density functional theory (DFT) [33,34]. The generalized gradient approximation in type Perdew-Burke-Enzerhof (GGA-PBE) was used. On the fly-generated pseudopotentials were implemented to enable the inclusion of core holes [35]. The cutoff energy was set at 500 eV. The structure used was a single layer cell consisting of 64 pairs of H and B atoms and optimized under three conditions: (i) $dE/\text{ion} < 2 \times 10^{-5}$ eV, (ii) $|F|_{\max} < 5 \times 10^{-2}$ eV/Å, and (iii) $|dR|_{\max} < 1 \times 10^{-3}$ Å. The values of the unit-cell parameters were taken from the literature [14,24]. The mesh size chosen for the Brillouin zone integral was $2 \times 2 \times 1$.

III. RESULTS AND DISCUSSION

Figure 2 presents an optical microscope image of the HB sheets at edges. The surface is widely flat and the edges are sharp. In contrast to the microscopic HB sheets [7], the HB atomic layers in the macroscopic sheet are unfolded and stacked upon each other. There are bright micron-size protrusions that may be ascribed to the extra HB microflakes agglomerated on the surface. The holes at the surface may correspond to defects in the sheet (see Appendix).

To examine atomic structure of the macroscopic HB sheet, the XRD pattern was taken (Fig. 3). Three distinct Debye–Scherrer rings, labeled i, ii, and iii, were observed; the corresponding peaks were found in the radial profile at $2\theta \sim 6°$. Using the Bragg equation, values of the atomic spacing were collected (Table I) along with those reported previously [7,11]. The results of the macroscopic HB sheet are consistent with those obtained from powders. Recalling the HB layer model [Fig. 1(a)], the previous research of the first-principles calculation [14] reported the structural parameters as $l_{\text{B-B}} = 1.7$ Å, $l_{\text{B-H-B}} = 1.8$ Å, and $h_{\text{H-B-H}} = 1.9$ Å. These values set the size of the unit cell as $a_0 = 3.0$ Å. The layer height h_0 may be evaluated by summing $h_{\text{H-B-H}}$ and twice the radius (r_{H}) of the hydrogen atom. Since r_{H} corresponds to the Bohr radius $(r_{\text{Bohr}} = 0.5$ Å), the HB layer height is estimated to be $h_0 \sim 2.9$ Å. From Table I, the atomic spacings of 5.8 Å, iii in Fig. 3, and 9.0 Å, i in Fig. 3, fairly match with $2h_0 = 5.8$ Å
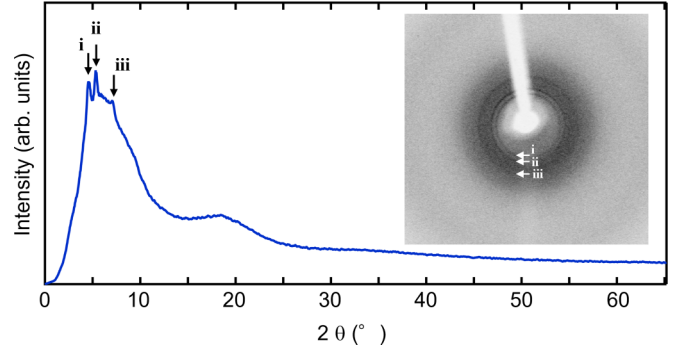

FIG. 3. Angular (2θ) dependence of the XRD intensity of the macroscopic HB sheet. The inset shows the XRD pattern. Labels i, ii, and iii indicate three prominent features of the three Debye–Scherrer rings.

and $3h_0 = 8.7$ Å, respectively. Most likely there is a stacking of HB layers of types ABAB and ABCABC. For the atomic spacing of 7.7 Å, ii in Fig. 3, the value also indicates the ABAB-type stacking but with a different interlayer distance. These facts indicate that there exist several types of layer stacking in the macroscopic HB sheet. Taking the Miller index (hkl) of h, k, and l for the intralayer and interlayer directions, respectively, the Bragg peak position at $2\theta \sim 6°$ may be assigned to (001) and the broad peak width features contributions from various stacking structures. Based on the intralayer lattice parameter a_0, the Bragg reflection at $2\theta \sim 19°$ corresponds to the Miller index of (011) or (101), for example, and the peak width is broadened because of the distribution in interlayer stacking. It is of note that the atomic structure of the HB layer has already been examined by transmission electron microscope and it has been confirmed to have the honeycomb structure, shown in Fig. 1(a) [7].

To conduct the spectral evaluation, we exploited the ease of preparing the macroscopic sheets on several substrates, as described in Sec. II A. We soaked a Ni wire mesh (30 mesh, aperture ratio: 68%) from the Nilaco Corporation (Tokyo, Japan) into the HB-containing solution [Fig. 1(c)], and fabricated the sheet on the mesh [Fig. 4(a)]. VIS-UV absorption spectroscopy was performed using the HB sheet sample on the Ni wire mesh. From the optical transmission spectra of the HB sheet in the VIS-UV [Figs. 4(b) and 4(c)] there are

TABLE I. Structure and XRD parameters for HB sheets, measured using x-ray tubes and synchrotron radiation (SR).

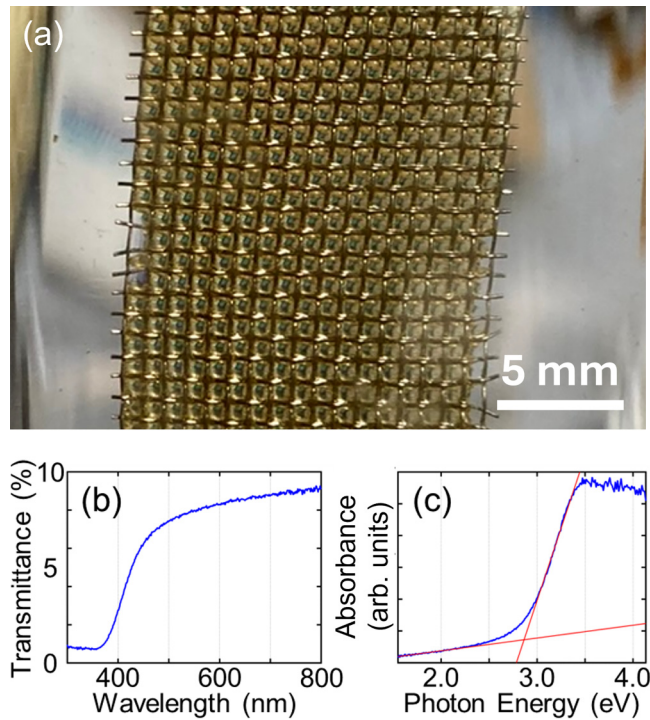| 2θ (°)	Light source	Atomic spacing (Å)	Note
27	Cu Kα	3.30	powder HB [36]
17.5	Cu Kα	5.07	powder HB
1.15	SR ($\lambda = 0.10713$ Å)	5.34	powder HB [11]
7.07	Mo Kα	5.76	macroscopic HB (iii in Fig. 3)
5.31	Mo Kα	7.67	macroscopic HB (ii in Fig. 3)
4.1	Ag Kα	7.8	powder HB [7]
4.55	Mo Kα	8.95	macroscopic HB (i in Fig. 3)

FIG. 4. VIS-UV absorption spectra measured by the transmission method. (a) Photographic image of the macroscopic HB sheets, prepared on a Ni wire mesh. VIS-UV spectra of (b) transmission and (c) absorbance. The red lines are linear extrapolations of the spectral features to evaluate the photon energy edge at the crossing point.
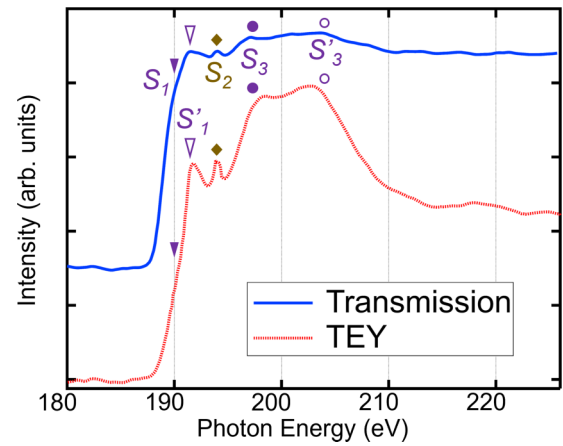

FIG. 5. X-ray absorption spectra of the macroscopic HB sheet. XAS spectra taken through two types of the signal detection: transmission (blue) and TEY (red) methods. The symbols indicate spectral peaks.

characteristic features around the 400 nm wavelength. Converting the transmission signal to an absorption energy, the spectral edge was found at the photon energy ($h\nu$) of 2.86 eV. The feature is consistent with the optical interband transition of the HB atomic sheet that was reported experimentally for the powder sample ($h\nu = 2.8$ eV) through diffuse reflection spectroscopy [24]. The spectral edge is also consistent with the band calculation ($h\nu = 2.4$ eV) [24].

XAS measurements have advantages in that the electronic states of a sample can be probed and that the results can be compared directly with a first-principles calculation. In general, there is a large optical absorption in a material in the x-ray region that covers the Boron K-shell absorption edge at $h\nu \sim 190$ eV. This optical property has hindered the XAS measurement in the transmission geometry. However, the present process, described in Sec. II A, provides the HB sheet sample on a Ni wire mesh that ensures the sheet is thin enough to detect the transmission signal. The transmission XAS spectrum at the B K-edge (Fig. 5), along with a reference spectrum taken by the TEY method, shows it to be consistent with that reported for a HB powder sample [14].

In the XAS spectra of the macroscopic HB sheet, the fine spectral structure is identifiable with notable features, labeled S_1, S_1', S_2, S_3, and S_3'. The S_2 peak at $h\nu = 194$ eV corresponds to boron species, such as boric acid or boron oxides, that have a B-O bond [14]. The peak intensity is much smaller than the spectra of the HB sample, reported previously [14], indicating the present spectra have better quality. The spectral shoulder, S_1, at $h\nu = 190$ eV appears clearer in the spectra taken by

the transmission method than that by the TEY method. Apparent peaks of S_1', S_3, and S_3' are observed at $h\nu = 191.5$ eV, 197.5 eV, and 203.5 eV, respectively. The features, S_1, S_1', S_3, and S_3', are likely ascribable to electronic states of the HB sheet. To examine the assignment, a spectral simulation was made based on the first principles. The calculated XAS spectra of the honeycomb-lattice type HB sheet [Fig. 1(a)] are shown in Fig. 6(a) with various orbital contributions of B $2p_x$, $2p_y$, $2p_z$, and their total summation. The B K-edge spectrum fall into two energy classes, S_a and S_b. Near the Fermi level (E_F), it is dominated by the $2p_z$ component, whereas, above $E - E_F = 6$ eV, there are apparent contributions from all the B $2p$ orbitals.

We display in Figs. 6(b) and 6(c) the wave function distributions of states at E_F for the honeycomb-lattice type HB sheet, which has a semimetallic band structure [14]. The distribution is in-plane ($2p_x$, $2p_y$) with the sheet for a hole-pocket band at the Γ point, whereas it is out-of-plane ($2p_z$) for an electron-pocket band at the Y point [14]. The dominant $2p_z$ component in the S_a region is ascribed to the state illustrated in Fig. 6(c) because the dispersion curve of an electron pocket extends energetically above E_F. The presence of this $2p_z$-derived state has also been observed for the diborane molecule. Figures 6(d) and 6(e) present the highest occupied molecular orbital (HOMO) and the lowest unoccupied molecular orbital (LUMO), calculated based on the density functional theory (see Appendix). The HOMO has an in-plane ($2p_x$, $2p_y$) character, whereas the LUMO has an out-of-plane ($2p_z$) character. Comparing the spatial distributions, Figs. 6(b) and 6(c) with 6(d) and 6(e), a wave function of the HB sheet can be described as a Bloch state of the molecular orbital of diborane. The model is consistent with that for borophane layers with pentagon/heptagon tiling [37] and with arguments regarding the 1D boron, bumulene [38,39].

Combining the experimental and simulated XAS spectra (Figs. 5 and 6) indicates that features S_1 and S_1' may be assigned to the $2p_z$ state in the S_a region. Incidentally, the S_1 state appears clearer in the spectrum taken by the (bulk-sensitive) transmission method than that by the
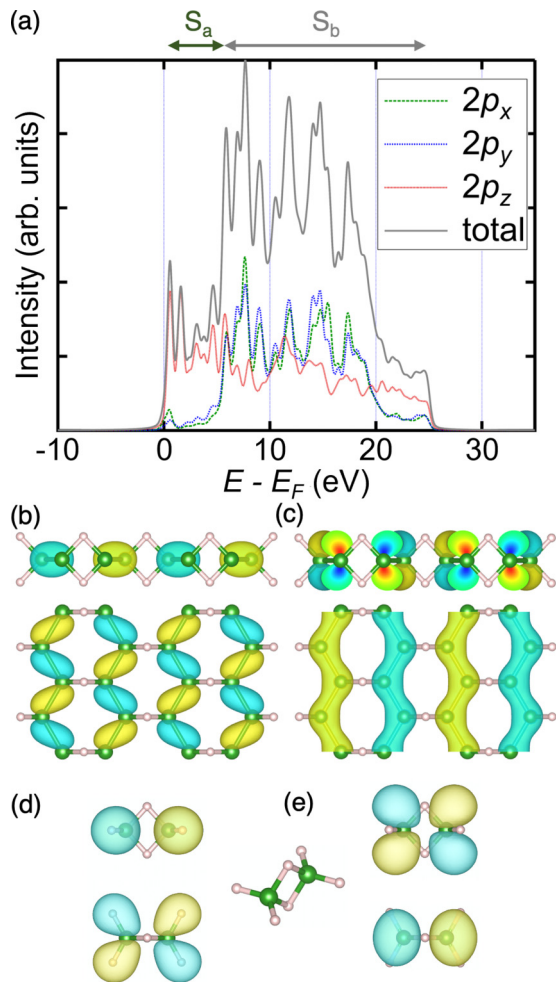
FIG. 6. Spectral simulations using first-principles calculations. (a) Simulated XAS spectra with the orbital convolutions, B $2p_x$ (green), B $2p_y$ (blue), B $2p_z$ (red), and total (black). Calculated energy was classified into two regions, S_a and S_b, for discussion. [(b), (c)] Wave function distributions of the bands at the Fermi level for the HB sheet [14] shown in Fig. 1(a). (b) A hole-pocket band at the Γ point and (c) an electron-pocket band at the Y point [14]. Molecular orbitals of diborane (d) HOMO and (e) LUMO. The molecular structure is presented in the figure. In (b)–(e), the color corresponds to signs of the wave functions or orbitals. Panels (b) and (c) were adapted with permission from Ref. [13].

(surface-sensitive) TEY method. The inference is that the B $2p_z$ state is sensitive to the possible adsorption of an external atom at the surface. Concerning the S_3 and S_3' features, the energy positions referred from the absorption edge match with the S_b energy region. These results indicate that the S_3 and S_3' states have B $2p_x$, $2p_y$, and $2p_z$ contributions and they may be assigned to antibonding states of the B and H atoms.

Measurements of the macroscopic HB sheet through the VIS-UV and x-ray spectroscopies have unveiled details of the electronic structure. Their consistency with HB powder data [7,14] indicate that these HB samples share the same unit as the HB atomic layer, as observed in XRD, as well as its electronic state. The fine spectral structures in the x-ray absorption spectra, the so-called near-edge x-ray fine structure, have been used as fingerprints of materials [32]. Recently, there have been growing interest in extending this method to machine-learning approaches to spectral analysis [40,41]. It has now become possible to deduce automatically various material information such as the atomic structure and bonding configurations, from x-ray absorption spectra. The experimental and simulated spectra in the present research play the role as input data for boron materials.

HB sheets have been found useful as a hydrogen transfer material or as chemical templates for catalytic reactions [20–24]. They have been proposed moreover to be utile in electrochemistry and (opto)electronics, for example [18–28]. The fabrication method, described in Sec. II, enables HB sheets of various sizes and morphologies, depending on the process step. The spectral evaluations show that the HB sample at each stage shares the same electronic states of the honeycomb-lattice type HB atomic layer. Therefore, optimized HB sheets can be designed and fabricated into desired areas and shapes for specific usage. Moreover, the present fabrication method enables sheets on different substrates to prepared, as demonstrated for a Ni mesh [Fig. 4(a)] and a Si wafer (see Appendix). The HB sheet can be set inside functional heterostructures and also worked as coating materials over surfaces or as adhesion junctions at interfaces. This simple fabrication process opens a wide range of applications in industrial fields for tailored HB sheets.

IV. CONCLUSIONS

In summary, we described the fabrication method of HB sheets of macroscopic scale and presented the evaluation using measurements obtained through several optical spectroscopies. Each sheet has a characteristic absorption in the infrared and visible region, consistent with reported data for powder samples, confirming the chemical bonds and the valence electronic states that are associated with hydrogen and boron atoms. X-ray spectra at the B K-shell absorption revealed the detailed electronic structure through a comparison with theoretical simulations on a honeycomb-lattice network. The macroscopic fabrication method and spectral data, presented in this research, open opportunities to develop the bottom-up methods for future applications of HB sheets. For example, the macroscopic HB sheet can be a source to fabricate a wide and unfolded HB layer by the appropriate exfoliation. It leads further to a potential to transfer it on a substrate and to prepare heterostructures with the other 2D materials. In the library of monatomic layers [1], the HB sheet likely becomes the significant one in academy and in industry.
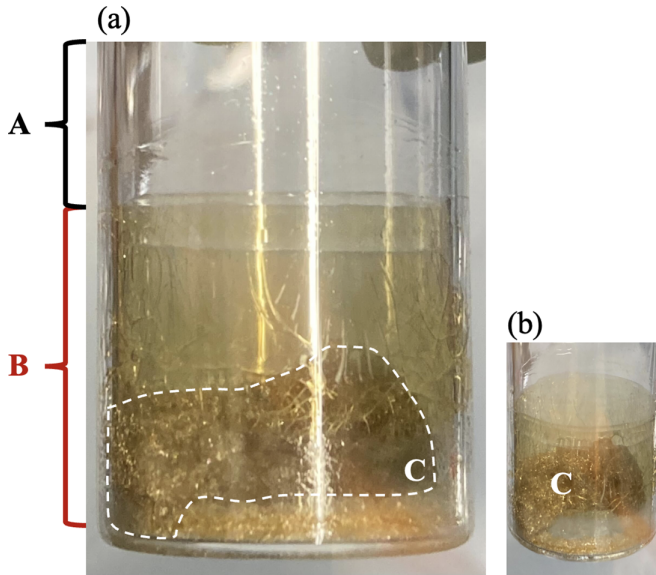
FIG. 7. Photographs of the HB sheets in a bottle after the heat treatment. A pristine wall and the HB sheet-coated wall are labeled A and B, respectively. An sediment is indicated by C.

APPENDIX A: DETAILED DESCRIPTIONS ON THE SYNTHESIS AND THE REFERENCE DATA

1. Raw HB sheets in a sample bottle

Figure 7 shows a photograph of the HB sheets in a sample bottle. The sheets are stuck inside a sample bottle. By peeling the sheets from the bottle wall, we took the HB sheet outside and stored them in a box, as shown in Fig. 1(d). As found in Fig. 7, one can find the yellow colored sheet on the wall (B) that is sharply contrast to the transparent wall of a bottle (A). Sediments (C) at the bottom are an assembly of HB flakes [7].

2. An infrared spectra of the HB Sheet

The HB sheet was characterized by Fourier Transform Infrared Spectroscopy (FT-IR). The measurement was made by the Attenuated Total Reflection (ATR) method using BRUKER ALPHA II. The spectrum is given in Fig. 8 with the peak assignments [7,11,24,42] and it can be used as the reference for the current research.
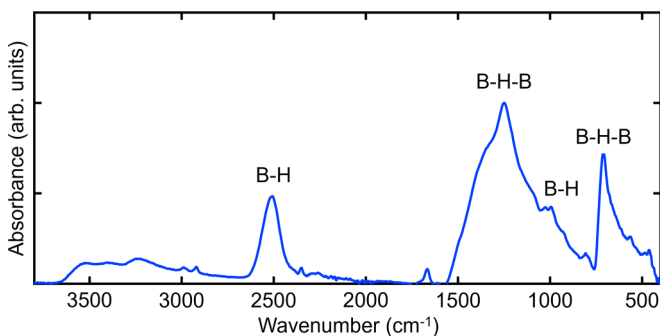

FIG. 8. FT-IR spectrum of the HB sheet with the peak assignment, based on the previous reports [7,11,24,42].
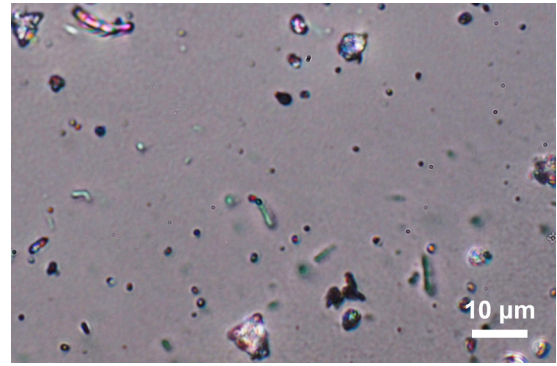

FIG. 9. An enlarged image of the HB sheet in Fig. 2.

3. Defects on the HB sheet

Figure 9 shows an optical image of the enlarged area of the HB sheet, shown in Fig. 2. Defects are micrometer sized and the density was evaluated 1.6×10^{10} m^{-2}.

4. Microscopic flakes of the HB sheet

Microflakes of the HB sheet were observed separately with an optical microscope (Fig. 10).

5. Fabrication on substrates

Macroscopic HB sheets were prepared on a substrate of a Si wafer an imaged using an optical microscope (Fig. 11). To enhance its visual appearance, the Si substrate is intentionally colored in purple (Fig. 11, inset) by growing a thin SiO$_2$ layer.
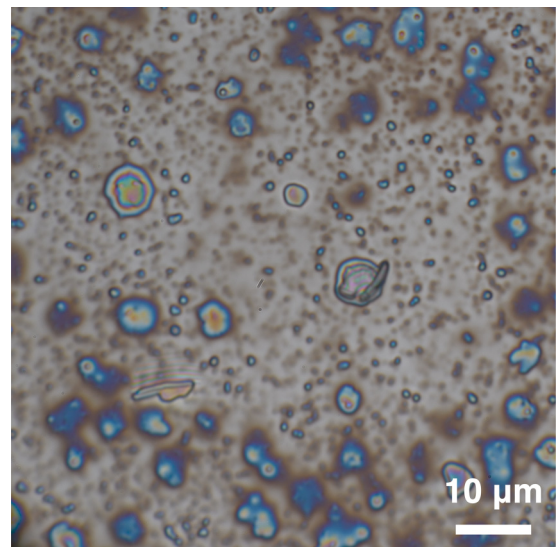

FIG. 10. An image of the microflake HB sheets, observed with an optical microscope. The micro-flake HB sheets are obtained by dropping a droplet of the volatile solvent in which HB sheets are dispersed onto a Si substrate, followed by spin coating. The HB sheets are observed as interference colors, while the residuals of solvent appear as gray grains.
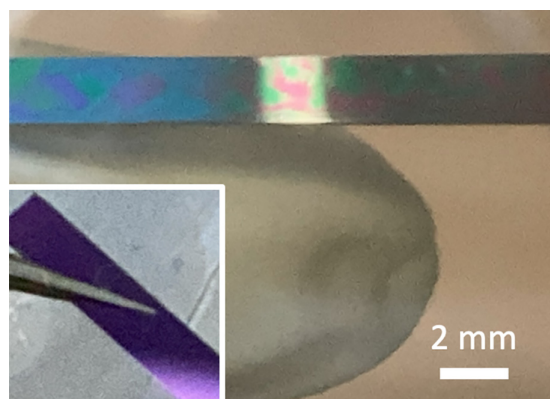
FIG. 11. An image of the HB sheet, coated on a Si wafer. The inset shows an image of the bare Si wafer. The HB sheet samples are observed as interference colors. A bright region at the center is a reflection of the light source.

The interference fringes indicate the presence of a coating of a HB sheet on the Si substrate.

6. Molecular orbital calculation

The structure optimization and molecular orbital calculations for diborane (Fig. 6) were performed using DFT implemented in the Python package Psi4 1.5.0 [43]. The Becke three-parameter Lee–Yang–Parr (B3LYP) method was used for the exchange-correlation functional calculations [44,45]. The Gaussian basis set 6-311g(d,p) was used to describe the electronic structure. The molecular geometry was optimized using the Gaussian level criterion. Atomic structures and wave functions were visualized using the VESTA program for visualization of electronic and structural analysis [46].

[1] I. Matsuda ed., *Monatomic Two-Dimensional Layers: Modern Experimental Approaches for Structure, Properties, and Industrial Use* (Elsevier, Amsterdam, 2018).

[2] S. Pinilla, J. Coelho, K. Li, and V. Nicolosi, Nat. Rev. Mater. **7**, 717 (2022).

[3] S. H. Choi, S. J. Yun, Y. S. Won, C. S. Oh, S. M. Kim, and K. K. Kim, Y. H. Lee, Nat. Commun. **13**, 1484 (2022).

[4] I. Matsuda and K. Wu (ed.), *2D Boron: Boraphene, Borophene, Boronene* (Springer, New York, 2021).

[5] Q. Li, V. S. C. Kolluru, M. Rahn, R. G. Hennig, P. Darancet, M. K. Y. Chan, and M. C. Hersam, Science **371**, 1143 (2021).

[6] Y. Xu, P. Zhang, X. Xuan, M. Xue, Z. Zhang, W. Guo, and B. I. Yakobson, J. Phys. Chem. Lett. **13**, 1107 (2022).

[7] H. Nishino, T. Fujita, N. T. Cuong, S. Tominaka, M. Miyauchi, S. Iimura, A. Hirata, N. Umezawa, S. Okada, E. Nishibori *et al.*, J. Am. Chem. Soc. **139**, 13761 (2017).

[8] X. Zhang, Y. Tsujikawa, I. Tateishi, M. Niibe, T. Wada, M. Horio, M. Hikichi, Y. Ando, K. Yubuta, T. Kondo, and I. Matsuda, J. Phys. Chem. C **126**, 12802 (2022).

[9] X. Zhang, M. Hikichi, T. Iimori, Y. Tsujikawa, M. Yuan, M. Horio, K. Yubuta, F. Komori, M. Miyauchi, T. Kondo, and I. Matsuda, Molecules **28**, 2985 (2023).

[10] T. A. Abtew, B. C. Shih, P. Dev, V. H. Crespi, and P. Zhang, Phys. Rev. B **83**, 094108 (2011).

[11] S. Tominaka, R. Ishibiki, A. Fujino, K. Kawakami, K. Ohara, T. Masuda, I. Matsuda, H. Hosono, and T. Kondo, Chem. **6**, 406 (2020).

[12] J. M. Oliva-Enrich, T. Kondo, I. Alkorta, J. Elguero, and D. J. Klein, ChemPhysChem **21**, 2460 (2020).

[13] I. Tateishi, X. Zhang, and I. Matsuda, Molecules **27**, 1808 (2022).

[14] I. Tateishi, N. T. Cuong, C. A. S. Moura, M. Cameau, R. Ishibiki, A. Fujino, S. Okada, A. Yamamoto, M. Araki, S. Ito, S. Yamamoto, M. Niibe, T. Tokushima, D. E. Weibel, T. Kondo, M. Ogata, and I. Matsuda, Phys. Rev. Mater. **3**, 024004 (2019).

[15] N. T. Cuong, I. Tateishi, M. Cameau, M. Niibe, N. Umezawa, B. Slater, K. Yubuta, T. Kondo, M. Ogata, S. Okada, and I. Matsuda, Phys. Rev. B **101**, 195412 (2020).

[16] M. Niibe, M. Cameau, N. T. Cuong, O. I. Sunday, X. Zhang, Y. Tsujikawa, S. Okada, K. Yubuta, T. Kondo, and I. Matsuda, Phys. Rev. Mater. **5**, 084007 (2021).

[17] A. A. Kistanov, Y. Cai, K. Zhou, N. Srikanth, S. V. Dmitriev, and Y. W. Zhang, Nanoscale **10**, 1403 (2018).

[18] Y. Jiao, F. Ma, J. Bell, A. Bilic, and A. Du, Angew. Chem. **128**, 10448 (2016).

[19] B. Mortazavi, M. Makaremi, M. Shahrokhi, M. Raeisi, S. Mostafa, V. Chandra, T. Rabczuk, and L. F. C. Pereira, Nanoscale **10**, 3759 (2018).

[20] A. Fujino, S. Ito, T. Goto, R. Ishibiki, J. N. Kondo, T. Fujitani, J. Nakamura, H. Hosono, and T. Kondo, ACS Omega **4**, 14100 (2019).

[21] A. Fujino, S. Ito, T. Goto, R. Ishibiki, R. Osuga, J. N. Kondo, T. Fujitani, J. Nakamura, H. Hosono, and T. Kondo, Phys. Chem. Chem. Phys. **23**, 7724 (2021).

[22] S. Ito, T. Hirabayashi, R. Ishibiki, R. Kawamura, T. Goto, T. Fujita, A. Yamaguchi, H. Hosono, M. Miyauchi, and T. Kondo, Chem. Lett. **49**, 789 (2020).

[23] T. Goto, S. Ito, S. L. Shinde, R. Ishibiki, Y. Hikita, I. Matsuda, I. Hamada, H. Hosono, and T. Kondo, Commun. Chem. **5**, 118 (2022).

[24] R. Kawamura, N. T. Cuong, T. Fujita, R. Ishibiki, T. Hirabayashi, A. Yamaguchi, I. Matsuda, S. Okada, T. Kondo, and M. Miyauchi, Nat. Commun. **10**, 4880 (2019).

[25] N. Ploysongsri, V. Vchirawongkwin, and V. Ruangpornvisuti, Vacuum **187**, 110140 (2021).

[26] Y. An, Y. Hou, H. Wang, J. Li, R. Wu, T. Wang, H. Da, and J. Jiao, Phys. Rev. Appl. **11**, 064031 (2019).

[27] C. Zhong, X. Li, and P. Yu, Commun. Phys. **7**, 38 (2024).

[28] J. Sun, Y. Zhang, J. Leng, and H. Ma, Physica E **97**, 170 (2018).

[29] T. Kondo, Chem. Lett. **52**, 611 (2023).

[30] S. Ito, M. Hikichi, N. Noguchi, M. Yuan, Z. Kang, K. Fukuda, M. Miyauchi, I. Matsuda, and T. Kondo, Phys. Chem. Chem. Phys. **25**, 15531 (2023).

[31] M. Sakurai, S. Morita, J. Fujita, H. Yonezu, K. Fukui, K. Sakai, E. Nakamura, M. Watanabe, E. Ishiguro, and K. Yamashita, Rev. Sci. Instrum. **60**, 2089 (1989).

[32] J. Stöhr, *NEXAFS Spectroscopy* (Springer, New York, 1992).

[33] M. D. Segall, P. J. D. Lindasn, M. J. Probert, C. J. Pickard, P. J. Hasnip, S. J. Clark, and M. C. Payne, J. Phys.: Condens. Matter **14**, 2717 (2002).

[34] S. J. Clark, M. D. Segall, C. J. Pickard, P. J. Hasnip, M. J. Probert, K. Refson, and M. C. Rayne, Z. Kristallogr. **220**, 567 (2005).

[35] S. P. Gao, C. J. Pickard, A. Perlov, and V. Milman, J. Phys.: Condens. Matter **21**, 104203 (2009).

[36] N. Noguchi, S. Ito, M. Hikichi, Y. Cho, K. Goto, A. Kubo, I. Matsuda, T. Fujita, M. Miyauchi, and T. Kondo, Molecules **27**, 8261 (2022).

[37] Y. Ando, T. Nakashima, Y. Heming, I. Tateishi, X. Zhang, Y. Tsujikawa, M. Horio, N. T. Cuong, S. Okada, T. Kondo, and I. Matsuda, Molecules **28**, 1225 (2023).

[38] Y. Tsujikawa, M. Horio, X. Zhang, T. Senoo, T. Nakashima, Y. Ando, T. Ozaki, I. Mochizuki, K. Wada, T. Hyodo, T. Iimori, F. Komori, T. Kondo, and I. Matsuda, Phys. Rev. B **106**, 205406 (2022).

[39] Y. Tsujikawa, X. Zhang, M. Horio, F. Komori, T. Nakashima, Y. Ando, T. Kondo, and I. Matsuda, e-J. Surf. Sci. Nanotechnol. **22**, 1 (2023).

[40] K. Shibata, K. Kikumasa, S. Kiyohara, and T. Mizoguchi, Sci. Data **9**, 214 (2022).

[41] T. Mizoguchi and S. Kiyohara, Microscopy **69**, 92 (2020).

[42] M. Hikichi, J. Takeshita, N. Noguchi, S. Ito, Y. Yasuda, L. T. Ta, K. I. M. Rojas, I. Matsuda, S. Tominaka, Y. Morikawa *et al.*, Adv. Mater. Interfaces **10**, 2300414 (2023).

[43] D. G. A. Smith, L. A. Burns, A. C. Simmonett, R. M. Parrish, M. C. Schieber, R. Galvelis, P. Kraus, H. Kruse, R. Di Remigio, A. Alenaizan *et al.*, J. Chem. Phys. **152**, 184108 (2020).

[44] A. D. Becke, J. Chem. Phys. **98**, 5648 (1993).

[45] C. Lee, W. Yang, and R. G. Parr, Phys. Rev. B **37**, 785 (1988).

[46] K. Momma and F. Izumi, J. Appl. Crystallogr. **44**, 1272 (2011).